ELSEVIER

Journal of Fluids and Structures 23 (2007) 101–115

JOURNAL OF FLUIDS AND STRUCTURES

www.elsevier.com/locate/jfs

Experimental investigation on splashing and nonlinear fingerlike instability of large water drops

S.S. Yoon[a,*], R.A. Jepsen[b], M.R. Nissen[c], T.J. O'Hern[d]

[a]*Mechanical Engineering Department, Korea University, Anamdong, 5-Ga, Sungbukgu, Seoul 136-713, Korea*
[b]*Mechanical Environments, Sandia National Labs, P.O. Box 5800, Albuquerque, NM 87185, USA*
[c]*Diagnostic Applications, Sandia National Labs, P.O. Box 5800, Albuquerque NM 87185, USA*
[d]*Thermal/Fluid Experimental Science, Sandia National Labs, P.O. Box 5800, Albuquerque, NM 87185, USA*

Received 3 October 2005; accepted 1 August 2006
Available online 13 October 2006

Abstract

The fluid physics of the splashing and spreading of a large-scale water drop is experimentally observed and investigated. New phenomena of drop impact that differ from the conventional Rayleigh–Taylor instability theory are reported. Our experimental data shows good agreement with previous work at low Weber number but the number of fingers or instabilities begins to deviate from the R–T equation of Allen at high Weber numbers. Also observed were multiple waves (or rings) on the spreading liquid surface induced from pressure bouncing (or pulsation) within the impacting liquid. The first ring is transformed into a radially ejecting spray whose initial speed is accelerated to a velocity of 4–5 times that of the impacting drop. This first ring is said to be "splashing," and its structure is somewhat chaotic and turbulent, similar to a columnar liquid jet surrounded by neighboring gas jets at relatively high impact speed. At lower impact speeds, splashing occurs as a crown-shaped cylindrical sheet. A second spreading ring is observed that transforms into fingers in the circumferential direction during spreading. At higher Weber number, the spreading of a third ring follows that of the second. This third ring, induced by the pressure pulsation, overruns and has fewer fingers than the second, which is still in a transitional spreading stage. Several important relationships between the drop impact speed, the spray ejection speed of the first ring, and the number of fingers of the second and third rings are presented, based on data acquired during a set of drop impact experiments. Issues related to the traditional use of the R–T instability are also addressed.

Keywords: Finger instability; Drop impact; Splashing; Kelvin–Helmholtz; Rayleigh–Taylor

1. Introduction

Drop impact phenomena are often encountered in raindrop impact and in numerous industrial applications such as inkjet printing, painting, spray-wall impact within the internal combustion-engine, and fire suppression sprays. We are particularly interested in fuel tank impact scenarios that lead to a high-speed large liquid slug impact (extremely high Weber number) and dispersion phenomenon, as shown in Fig. 1 (Jepsen et al., 2004) where a thin-walled aluminum

*Corresponding author. Tel.: +82 2 3290 3376; fax: +82 2 926 9290.
E-mail address: skyoon@korea.ac.kr (S.S. Yoon).

0889-9746/$ - see front matter © 2006 Elsevier Ltd. All rights reserved.
doi:10.1016/j.jfluidstructs.2006.08.009

Fig. 1. Dispersed water (dyed red) at furthest extent radially from impact (Jepsen et al., 2004). Frame is approximately 92 m wide and was acquired 2 s after impact.

tank filled with red-dyed water (2830 kg) impacts an unyielding wall at the speed of 100 m/s. Upon impact, the tank immediately peeled away from the water slug, leaving a bare mass of water to impact the target. The Weber number for this case is on the order of $\sim 10^8$ which far exceeds the previously reported studies limited to $\mathrm{We} = \rho D U_{\mathrm{imp}}^2/\sigma < 5 \times 10^4$, where ρ, U_{imp}, D, and σ are the liquid density, impact speed, drop diameter, and the liquid surface tension. There is an extensive literature containing relevant work, but at lower Weber number. The previous relevant work is included in Worthington (1877), Allen (1975, 1988), Chandra and Avedisian (1991), Prosperetti and Oguz (1993), Rein (1993), Fukai et al. (1993), Mundo et al. (1995), Yarin and Weiss (1995), Pasandideh-Fard et al. (1996), Marmanis and Thoroddsen (1996), Mao et al. (1997), Cossali et al. (1997), Thoroddsen and Sakakibara (1998), Weiss and Yarin (1999), Rieber and Frohn (1999), Bussmann et al. (2000), Kim et al. (2000), Aziz and Chandra (2000), Davidson (2000, 2002), Thoroddsen (2002), Rioboo et al. (2002), Sikalo et al. (2002), Manzello and Yang (2002), Roisman et al. (2002), Sivakumar and Tropea (2002), Rozhkov et al. (2002), Renardy et al. (2003), Josserand and Zaleski (2003), Mehdi-Nejad et al. (2003), Roux and Cooper-White (2004), Thoroddsen et al. (2004), Mehdizadeh et al. (2004), Ge and Fan (2005), and Xu et al. (2005), of which details will be discussed later.

The need to investigate liquid impact at extremely high Weber number provides a unique opportunity to collect data not observed and analyzed in previous work. However, these large-scale tests (Fig. 1) are difficult to repeat and to instrument with the diagnostics necessary to measure details of the fluid structure during break-up and dispersion. Therefore, several smaller scale tests were performed to investigate the impact and break-up phenomena for large water drops or slugs ($\sim$0.1 m diameter) at large Weber number (1×10^4–1×10^6). This scale still requires a delivery mechanism such as a thin-walled bladder or tank to keep the liquid mass intact prior to impact. This necessity adds a disturbance to the water slug surface not otherwise seen in smaller, smooth drops. The effects of this disturbance will be discussed in further detail. The range of Weber number for the experiments presented here were chosen to (i) repeat previous work and compare the test apparatus and procedure at low Weber number and (ii) extend the experiment to the highest possible Weber number within the bounds of the test equipment.

Our experiments show that upon impact the spreading liquid surface forms several waves or rings. The first ring, defined as "splashing," is transformed into a radially ejecting spray whose initial speed is accelerated to a velocity of 4–5 times that of the impacting drop. A second spreading ring transforms into fingers in the circumferential direction during spreading. At higher Weber number, a third ring follows that of the second. This third ring, induced by pressure pulsation, overruns and has fewer fingers than the second, which is still in a transitional spreading stage.

As per well-known classical experiments (Worthington, 1877), a drop is known to stick to the impacting surface at a relatively high impact Weber number when the drop surface tension energy is not high enough to overcome the drop's dissipative energy (Aziz and Chandra, 2000). Upon sticking, the drop spreads radially and forms a toroidal ring (which we define as the 2nd ring; the previous paragraph defines the "rings") at a relatively low Weber number. At an intermediate Weber number, an azimuthal instability develops and forms "fingers" at the rim of the spreading ring. If

the Weber number is increased even more, the drop "splashes" (which we define as the 1st ring) at the first contact with the surface prior to the finger formation. Here, we distinguish the definition of "drop" from that of "droplet"; the drop is the falling drop (whose size is relatively large) prior to impact, while the droplet is the splashed droplet (whose size is relatively small) subsequent to the impact. Splashing plays a significant and dominant role in the drop impact at extremely high impact speed as in Fig. 1; only splashing occurs without any spreading.

Several fundamental questions remain regarding the drop impact phenomenon. What causes the splashing and finger formation at the edge of the spreading ring? It is certainly fair to ask, "Is it possible to predict the number of fingers using a linear theory?"

The classical Rayleigh–Taylor (R–T) instability (Chandrasekhar, 1961; Allen, 1975; Sharp, 1984; Youngs, 1984; Read, 1984; Aref and Tryggvason, 1984; Clark, 2003) in which heavy fluid decelerates toward a light fluid, is known to appear as fingers at the fluid–fluid interface: the R–T instability occurs when the normal vector projected from the heavy fluid surface is in the opposite direction to the acceleration, i.e., the interface between heavy and light fluids is accelerated. Allen (1975) suggested that the observed fingers at the front of the ring of liquid spreading after drop impact were caused by the R–T instability due to the radial expansion of the liquid into the surrounding air. For the past three decades, Allen's idea was well accepted within the community. However, the question remains: What causes the splashing that occurs prior to spreading at high Weber number?

The wavenumber corresponding to the maximum growth rate, ω, of the R–T instability is as follows:

$$k^2 = \frac{g(\rho_2 - \rho_1)}{3\sigma}, \tag{1}$$

where g is the acceleration, ρ_1 and ρ_2 the air and fluid density, respectively, and σ the fluid surface tension (Allen, 1975). However, the images in Fig. 2 (Xu et al., 2005) indicate that there is no unstable mode in the experiment for the limiting case $\rho_1 \to 0$ ("vacuum"). However, the mode of the R–T theory suggests that the interface should be still unstable so long as the surface tension remains constant; the experiment of Xu et al. (2005) and the R–T theory do not agree. Note that σ does not vary substantially due to atmospheric pressure variation [see Hansen and Rodsrud (1991)]. Certainly, the R–T theory cannot explain the phenomenological behavior of the absence of splashing and finger formation shown in the experiment of Fig. 2. Had the R–T theory yielded the imaginary growth rate ($\omega^2 < 0$), the theory would have been consistent with experimental observation. Moreover, the wavelength ($\lambda = 2\pi/k$) of the R–T theory is not sensitive to small density differences (i.e., $\Delta\rho = 1000$ and 999), while the experiment shows that a density difference of 1 part in 1000 is important because of the air pressure (see Fig. 2). Also, from Fig. 2, the drop in the atmospheric pressure is slightly deformed just prior to the impact while the drop shape in the reduced atmospheric pressure does not seem to be affected.

It appears as though finger formation is the result of splashing whose disturbance provides an initial perturbation; when there is no splashing there is no finger formation, and vice versa. Xu et al. (2005) stated that splashing occurs because of compressed air while the initially contacted liquid rim flows outward but is pushed back by air resistance, deflecting its motion and resulting in added momentum in the vertical direction. The new explanations by Xu et al. (related to the collapsing/escaping air) better describe the mechanisms of splashing and the subsequent finger formation than the arguments deduced from the R–T instability (Allen, 1975).

Considering the shear effect of air, we have taken the limit of $\rho_1 \to 0$ for the case of vacuum to be consistent with the experiment of Xu et al. (2005). In this case, the wavenumber of the Kelvin–Helmholtz instability indicates that the mode is indeed stable as $k_{\max} \to 0$ in the limit of $\rho_1 \to 0$, which is consistent with the Xu et al. observation. The growth rate, ω, (which becomes imaginary when $\rho_1 \to 0$ and, thus, the flow is stable) and the wavenumber corresponding to the maximum growth rate, $k_{\max}$, of the Kelvin–Helmholtz are as follows:

$$\omega^2 = \frac{\rho_1}{\rho_2} U_{\mathrm{rel}}^2 k^2 - \frac{\sigma}{\rho_2} k^3, \quad k_{\max} = \frac{2\rho_1 U_{\mathrm{rel}}^2}{3\sigma}, \tag{2}$$

where U_{rel} is the relative velocity between the gas and liquid. Fig. 3 shows that the Kelvin–Helmholtz theory can explain the quickly changing characteristics of the instability mode as the gas density changes from $\rho_1 = 1$ to $\rho_1 \to 0$, while the R–T theory cannot explain this sudden change. The experiment of Xu et al. (2005) indicates that a sudden change in stability mode is observed when the gas density changes from $\rho_1 = 1\,\mathrm{kg/m^3}$ to $\rho_1 \to 0$. Since most previous liquid impact tests have been conducted under atmospheric conditions where the gas density is $1\,\mathrm{kg/m^3}$ (whose region is coincidentally shared by both the R–T instability and the Kelvin–Helmholtz instability as shown in Fig. 3), it may have been coincidence that the experimental data were in agreement with the prediction deduced from the R–T theory. Therefore, it is certainly fair to further investigate the applicability of the R–T theory for predicting liquid splashing and finger formation.

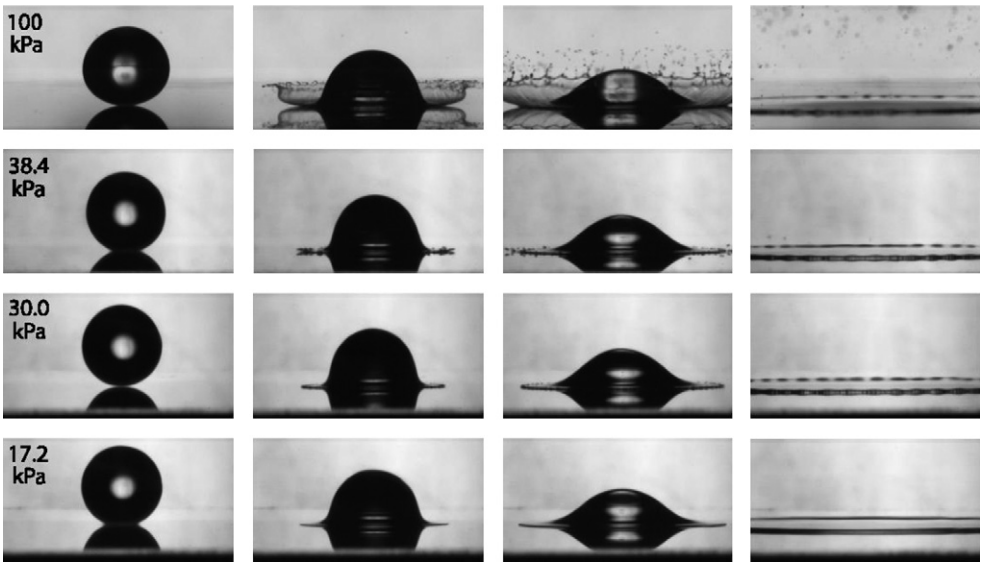

Fig. 2. Recent experiment by Xu et al. (2005). Neither the splashing nor finger formation occurred when the atmospheric pressure decreased. Reprinted with the permission of Prof. Sidney R. Nagel of the University of Chicago.

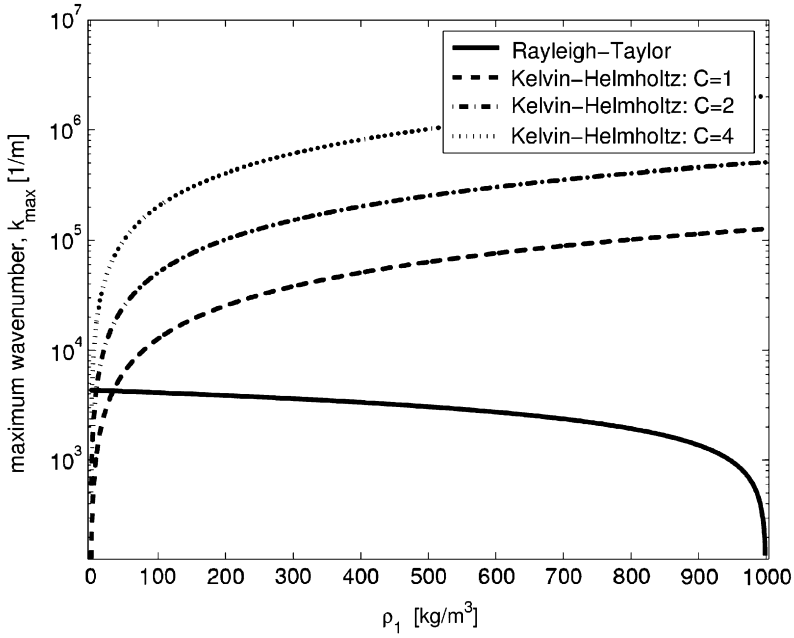

Fig. 3. Maximum wavenumber comparison between the Rayleigh–Taylor and Kelvin–Helmholtz theories at various gas density, ρ_1. The drop examined by Xu et al. (2005) is considered for this comparison: the drop diameter is 3.4 mm, the impact speed is 3.74 m/s. For the Rayleigh–Taylor instability, the deceleration is approximated as $g \approx U_{\text{imp}}^2/D$ according to Aziz and Chandra (2000). For the Kelvin–Helmholtz instability, the ratio between the air escaping speed and the impact speed is taken to be $C = U_{\text{rel}}/U_{\text{imp}} = 1$, 2, and 4.

Here, we present our experimental data which agree well with the previously published experimental data at low Weber number (Aziz and Chandra, 2000; Mehdizadeh et al., 2004), but deviate from the R–T theory at very large Weber number, consistent with our proposed scenario that the R–T theory was coincidentally used and thus incorrectly validated. Our experiments also show the high induced velocities of the escaping air and splashing from the drop impact, which indicate strong shear-driven interaction and momentum transfer between the impacting liquid and the surrounding air.

2. Experimental set-up

Large water slug impact experiments were done using latex bladders (balloons) to transport the slugs to a clear acrylic target (Fig. 4). Immediately prior to impact (8 cm) the latex was removed using a small (0.5 cm) blade. The latex peels away from the water in approximately 1 ms resulting in a large spherical water drop shaped like the latex bladder. The bladder is completely removed from the water when the drop impacts the target.

Data was gathered using three digital Phantom cameras (Vision Research, Wayne, NJ) arranged as shown in Fig. 4 with frame rates between 4800 and 10 000 fps and exposure times from 5 to 100 μs/frame. The cameras were synchronized using a single trigger. Both forward and backlighting techniques were used. Only forward lighting from directly underneath the target was used for processing the finger counting since it provided the sharpest visual images of the liquid air interface. Backlighting was generally used for side views and tracking droplets. In addition, a thin barrier with a 1×4 cm aperture at the impact surface was used to isolate a narrow slice of the flow in some of the tests, as shown in Fig. 4. *TrackEye* software was used to post-process the flowing liquid film and splashing for angle and velocity measurements.

Drop size and drop height were varied in order to cover a range of impact velocities and Weber number. Multiple tests (4–5 runs with constant droplet size) per fixed height were conducted to yield statistically reliable data. Approximately 10–15 tests were conducted for each Weber number. The number of fingers counted for each Weber number case had a less than $\pm 15\%$ standard deviation from the mean of each set of counts.

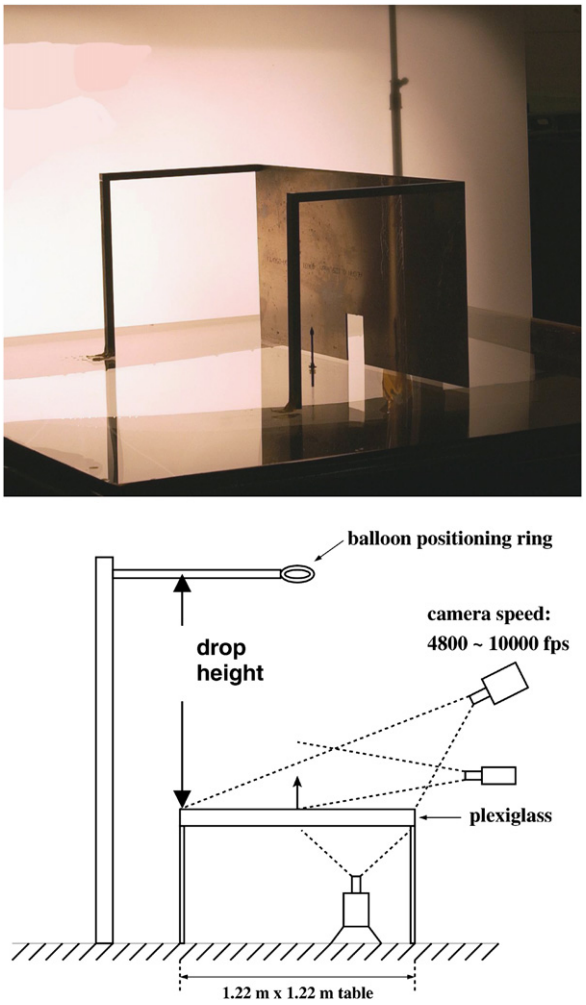

Fig. 4. Experimental set-up: blade is installed in the center of the 1.22 m × 1.22 m plexiglas. An aperture is placed to capture the characteristics of the initially ejected splashed droplets.

3. Results and discussion

When a drop impacts the surface, splashing (which is defined as the 1st ring; see Section 1) occurs followed by the spreading of the 2nd and possibly 3rd rings of the pressure pulsation. The finger formation of the 2nd ring involves a relatively smaller length scale (compared to that of the 3rd ring) and, thus, more fingers appear at the edge of the spreading rim. The 3rd ring (which is induced by the pressure pulsation) eventually overruns the 2nd ring (the initial spreading) and results in finger merging at the spreading edge. As a result, a thick and clear finger formation is seen as in Fig. 5 where a forward lighting technique was used. In this figure, finger formation is clearly shown in the snapshot, looking straight up from beneath one quadrant of the transparent impact surface. It is assumed that the number of fingers is uniformly distributed and, thus, the total number of fingers is four times the number measured in the quadrant surface.

When a balloon hits the blade in the plate center, the latex skin disrupts the surface of the drop and causes some atomization due to the shear stress (see Fig. 6). However, the spherical drop retains its original shape prior to contact with the surface. It is interesting to note that this necessary initial perturbation due to the latex skin-peeling does not seem to affect the core mechanisms of splashing and fingering because our experimental data for the low Weber numbers is in very good agreement with the previously reported data (Mehdizadeh et al., 2004) that was obtained using a smooth droplet without any latex around it (data comparison will be made later). Our observations also show that the drop's collapsing speed (the speed at which the top of the drop approaches the impact surface) is always less than the impact speed. This is because the drop is pushed in the opposite direction to the flow because of the nature of the incompressible elliptical flow prior to the period of collapsing, and because pressure bouncing impedes the downward collapsing motion. Multiple waves appear on the free surface flow during spreading. Many subscale waves are observed but we have identified the dominant two waves, defined as the 2nd and 3rd rings (it is recalled that the 1st ring was labeled "splashing") for a sphere liquid impact. Normally, the 3rd ring is not generated when the Weber number is not sufficiently high (i.e., $We < 5000$). It is suspected that pressure bouncing occurs because of the competition between the kinetic and surface tension energies. While the drop is spreading and ejecting subsequent to impact, due to the kinetic and potential energy converting into dissipative energies, the surface tension force tends to impede the energy conversion process, resulting in pressure bouncing. A case in point is manifest in Fig. 7 which shows the multiple radial waves appearing (more than 3) when a column liquid jet impacts on a transparent impact surface (photo taken straight up from beneath the transparent impact surface). This pressure bouncing has not yet been reported in the literature and, thus, the previous authors did not distinguish the 2nd and 3rd rings.

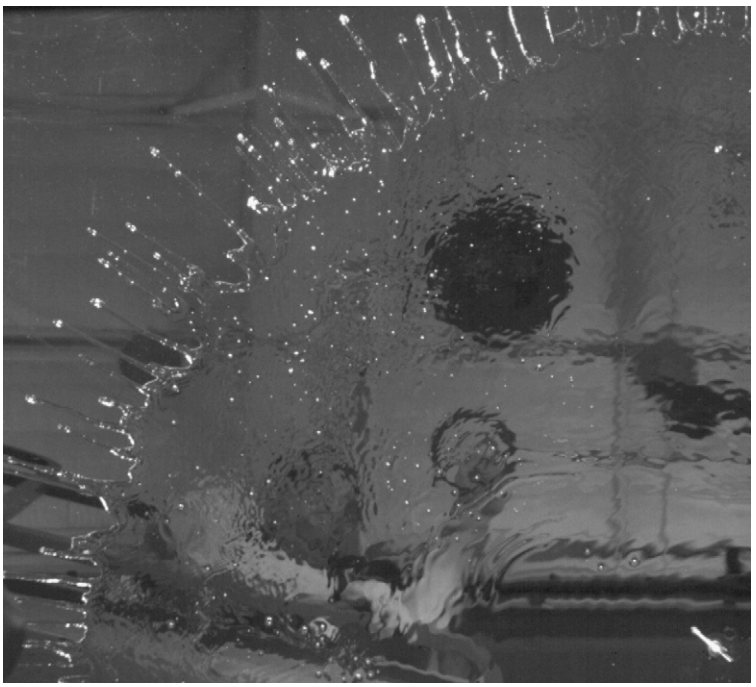

Fig. 5. Finger formation (3rd ring) at the quadrant surface (bottom view). $U_{imp} = 5\,m/s$, $D = 0.09\,m$.

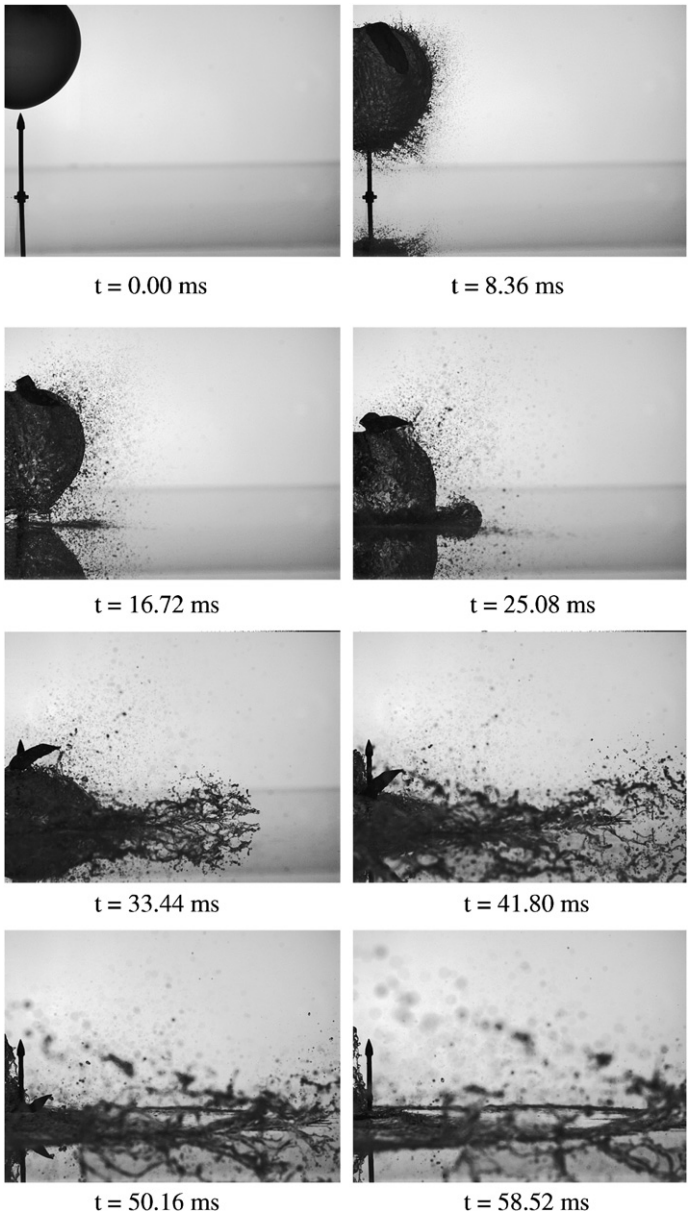

Fig. 6. Time evolution of an impacting droplet (taken at every 40 frames from a 4800 fps camera) from side-view. The operating conditions are $U_{imp} = 5.6\,m/s$, $D = 0.11\,m$. The droplet collapsing rate is estimated to be approximately 2.6 m/s.

Fig. 8 shows the time evolution of an impact from the bottom camera using a backlighting technique. The initially separated droplets from splashing have a speed about four times the impact speed, as indicated in Fig. 9. Here, it is recalled that the "droplets" were previously defined as the splashed droplets, not the main "drop", which is the falling primary drop. The only way for these separated droplets to obtain the momentum is from the air which is accelerated by a falling drop. Thus, there is a chain-reaction occurrence between the falling liquid drop and air.

The radial velocities of small droplets ejected during impact, measured by tracking the droplets using the *TrackEye* software, are shown in Fig. 9(a). Note that the total speed will generally be higher than this radial velocity. The initially separated droplets move the fastest, while those that follow move more slowly because they have experienced the necking (or stretching) effect of the capillary force which tends to impede the droplet's dynamic motion. The data labeled splash A, B, and C in Fig. 9 are from splashed droplets randomly selected to record their history of the radial

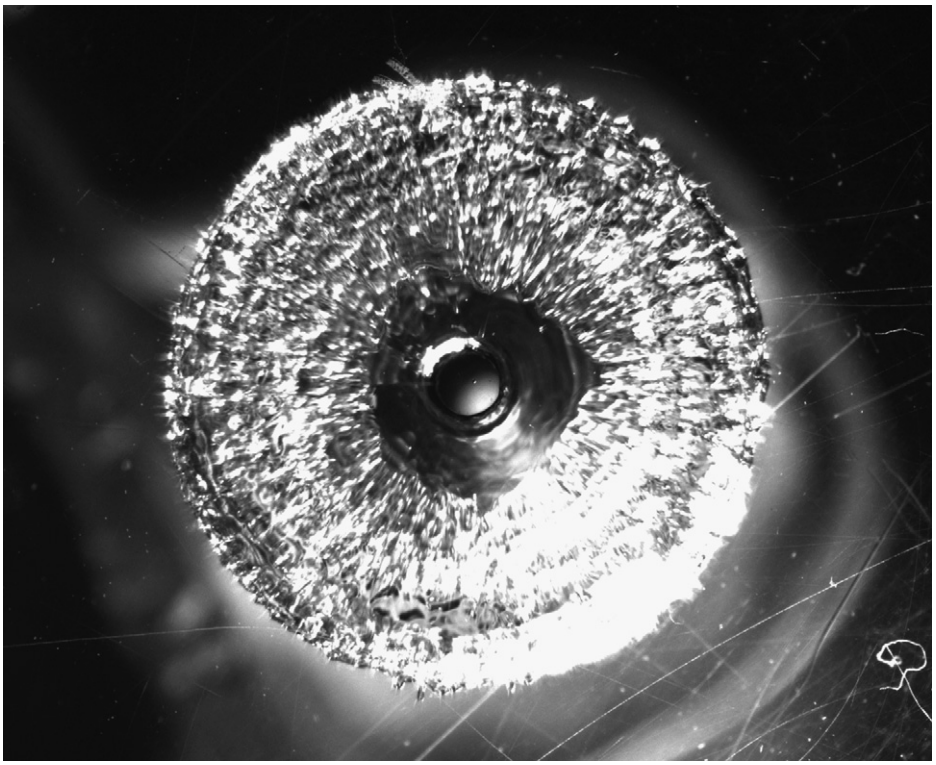

Fig. 7. Radially-induced multiple waves due to pressure pulsation when a column of liquid jet is continuously impacting on the plexiglass surface. Photo was taken from underneath location by Prof. Sanjeev Chandra's group of University of Toronto. Courtesy of Prof. Sanjeev Chandra.

velocity. All atomized droplets experience an aerodynamic drag subsequent to their separation; therefore, their speed is reduced while traveling, as indicated in Fig. 9(a).

The speed of the spreading 2nd ring from a 5 m/s impact fluctuates from 7 to 10 m/s for the time interval 27 ms $< t <$ 44 ms from Fig. 9(a) (see "2nd ring"). The velocity fluctuation is probably due to multiple waves surging toward the ring edge. Based on this fact, it is difficult to imagine that the fingers are due to the R–T instability because there is no apparent acceleration or deceleration.

As can be seen in Fig. 6, the mechanism of splashing is highly *nonlinear*, up to the level at which the flow is considered turbulent. Thus it may not be applicable to predict the final finger number using the linear theory of the R–T instability. The ejecting jets, somewhat similar to a spider-web in shape from the top-view, are always accelerated by some mechanism. Fig. 10 is a close-up view of the drop impact with lower impact speed than in Fig. 6, allowing more detailed information on the ejecting fluid under the fixed camera speed. Fig. 11, which corresponds to the radial velocity of the splashing droplets in Fig. 10, indicates that droplet acceleration occurs from $t = 5$ to 10 ms after impact. This is the same time period in which the wedge-shaped air volume between the drop and target collapses (Fig. 10). This phenomenon demonstrates that the escaping air accelerates the radially expanding fluid and could induce vertical momentum due to the air's vortex motion. After $t = 10$ ms, the front of the ejecting splashed droplets becomes obscured and the continuous measurement for the velocity using the *TrackEye* software was not possible. Therefore, several new tracking points were initiated at $t > 10$ ms (i.e., splash C–splash G) as in Fig. 11. Some droplets (i.e., splash 6 and 7) were still accelerating moderately when other droplets were decelerating due to the aerodynamic drag opposing the dynamic motion of the splashed droplet.

We claim that the collapsing/escaping air causes splashing, based on our experimental data showing that the initial spreading speed (U_{sp}) and the ejection speed (U_{eject}) are always much greater than the impacting speed (U_{imp}). This behavior can be explained *only* by some external force, in this case the air that is compressed under the falling slug (or drop) then is accelerated outward as the slug approaches the surface. It may be argued that the substantial air compression does not occur at this low Mach number. However, we believe that even moderate air compression causes the instability whose disturbance is large enough to result in splashing and the subsequent finger formation. The

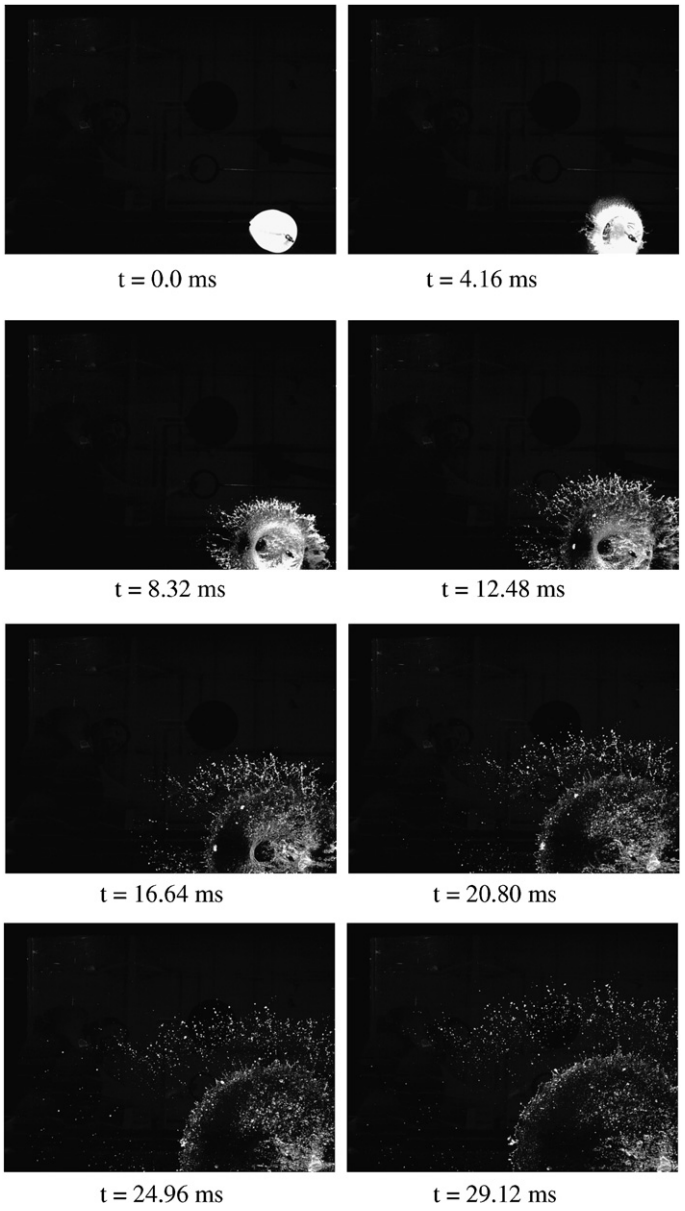

Fig. 8. Time evolution of the impacting droplet (taken at every 20 frames from a 4800 fps camera) at the quadrant surface (bottom view). The operating conditions are $U_{imp} = 5\,m/s$, $D = 0.106\,m$.

observations of Xu et al. (2005) (see Fig. 2), through another experimental method, support the importance of air on the splashing and fingering behavior.

For the case of liquid ejection due to splashing, escaping air accelerates the impacting liquid whose volume is comparable to the volume of the escaping air, based on our experimental observation as shown in Fig. 12. Upon impact, a crown-shaped cylindrical sheet initially arises in the direction of the air trajectory (see Figs. 2 and 6 for laminar and turbulent cases, respectively). Droplets are ejected (or separated) from the parent sheet because the incoming sheet speed cannot keep up with the initially accelerated speed of the crown edge/top. Thus, necking occurs and droplets are separated from the parent sheet. Finally, a finger appears as a result of the initial disturbance of splashing. If the initial disturbance had been suppressed by suppressing the splashing, the fingers would not have appeared at the spreading edge of the rim (see Fig. 2 for the case of the atmospheric pressure is 17.2 kPa). Thus, it is clear that the initial disturbance due to splashing is the fundamental cause of the fingering, rather than the R–T instability.

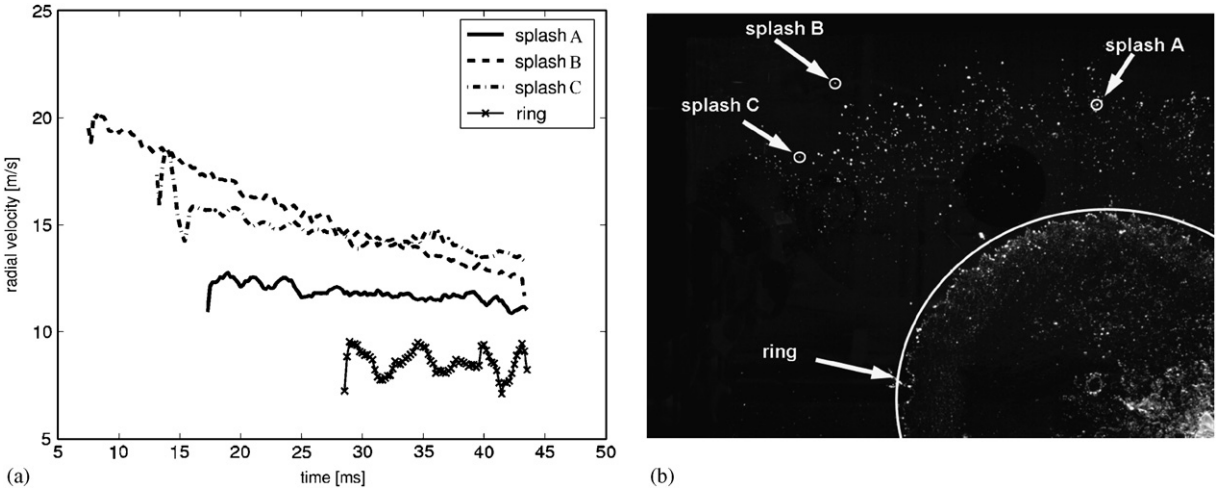

Fig. 9. (a) The droplet radial velocity. The operating conditions are $U_{\text{imp}} = 5\,\text{m/s}$, $D = 0.106\,\text{m}$. (b) The corresponding figure with respect to plot (a) indicating where the velocity measurements were taken.

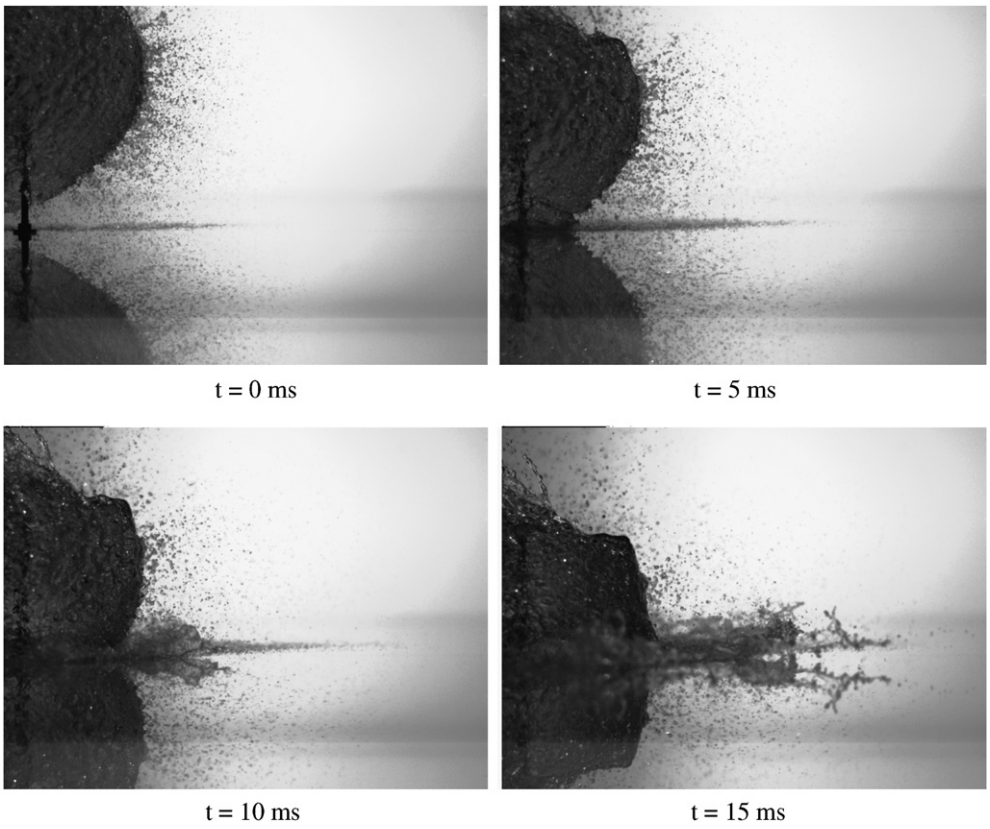

Fig. 10. Time evolution of an impacting droplet (taken at every 24 frames from a 4800 fps camera) from side-view. The operating conditions are $U_{\text{imp}} = 3.5\,\text{m/s}$, $D = 0.097\,\text{m}$.

In Fig. 13, the experimental data is not in agreement with $N_f = \text{We}^{1/2}\,\text{Re}^{1/4}/(4\sqrt{3})$ (Aziz and Chandra, 2000) whose analysis is based on the R–T instability of Allen (1975) (note that $\text{Re} = U_{\text{imp}}D/\nu$ where ν is the fluid kinematic viscosity). However, the experimental data is in better agreement with the later analysis of Mehdizadeh et al. (2004) that $N_f = 1.14\,\text{We}^{0.5}$. We have distinguished the 2nd and 3rd ring data in Fig. 13; the number of fingers in the 3rd ring is less

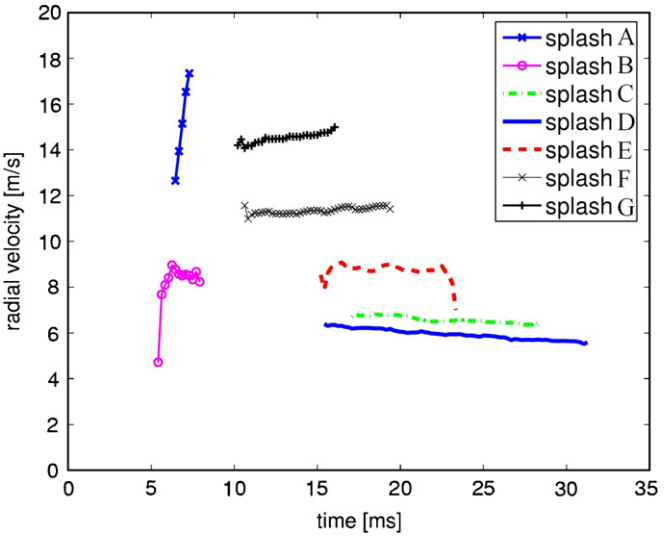

Fig. 11. The droplet radial velocity conjunction with Fig. 10. The initially-splashed droplets are accelerated from $t\sim5$ to ~8 ms (see Fig. 9).

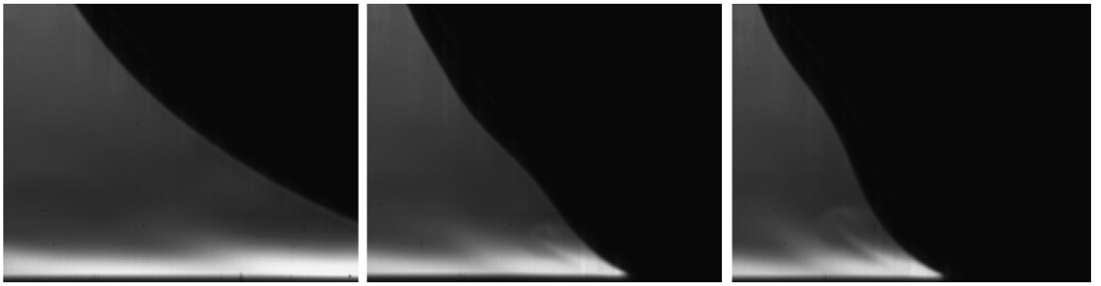

Fig. 12. Development of the vortex roll-up motion while air being compressed due to a falling drop.

than that of the 2nd because finger merging occurs when the 3rd ring overruns the 2nd. The data for two different drop masses show that differences in drop mass seem to result in different numbers of fingers at a constant Weber number. The difference is outside of the error tolerance and the pattern is consistent for the 2nd and 3rd rings. It is believed that the influence of droplet size, D, does matter, but not as the R–T theory suggests, i.e., the finger number N is proportional to $D^{0.75}$ according to the R–T theory. It is noteworthy to reiterate the fact that our current data at lower Weber number are in very good agreement (see "■" symbol in Fig. 13 for the 4 mm drop size data) with the previously reported data (Mehdizadeh et al., 2004) and in fact the data in Mehdizadeh et al. (2004) also begins to deviate slightly with the same trend reported here at the higher Weber number. Fig. 15 shows an additional qualitative data, which is indicative of the validity of our experimental data at low Weber number. Here, the Weber number applied is We $\sim$54 and the capillary number is $\mathrm{Ca} = \mu U_{\mathrm{imp}}/\sigma = 0.01526$. Thus the operating regime of the current data is in the regime proposed by Renardy et al. (2003) for the formation of the pyramidal surface structure; We Ca <2. It should be noted that the Weber number was previously defined with the drop's diameter in this report while Renardy et al. (2003) used the drop's radius for the Weber number definition.

It is interesting that the pattern of the finger number shown in Fig. 13 resembles that of the wavenumbers of the Kelvin–Helmholtz shown in Fig. 3. Here, the finger number should be proportional to the wavenumber of the linear theory if the theory (either the R–T or the Kelvin–Helmholtz theory) were to be applied. We propose the empirical formula that fits the experimental data what was until now published in the literature (including our current data),

$$N_f = -92 + 57\log(\mathrm{We}). \tag{3}$$

While being erudite in the fundamental cause of the finger formation, we ask two questions. First, why did previous authors not observe that the R–T instability was not capable of predicting the accurate number of fingers? Second, why

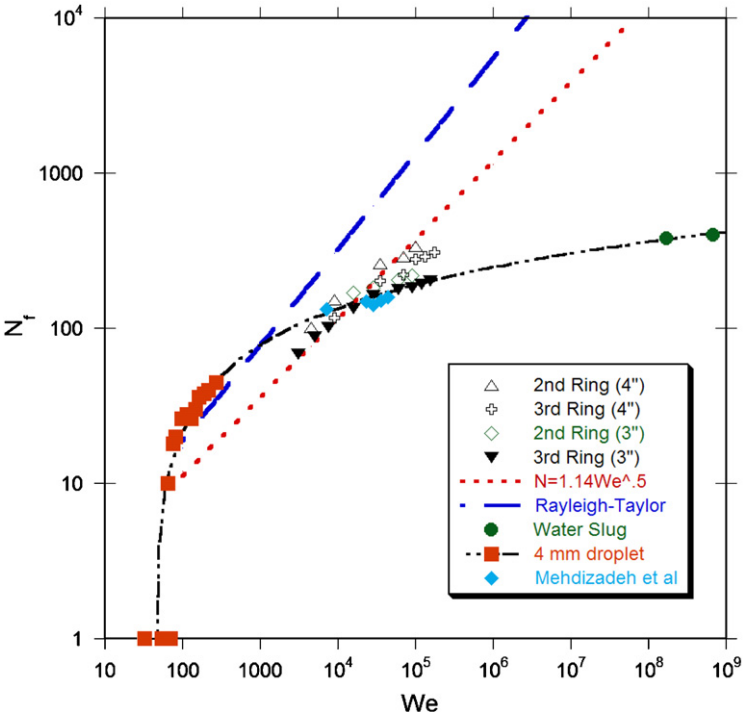

Fig. 13. The finger number at various Weber numbers. The finger number at the 2nd and 3rd rings are distinguished. Error estimation was found to be less than 15%, which is smaller than the size of the symbols. The symbol, "●" represents the water slug data of Jepsen et al. (2004) (see Fig. 1).

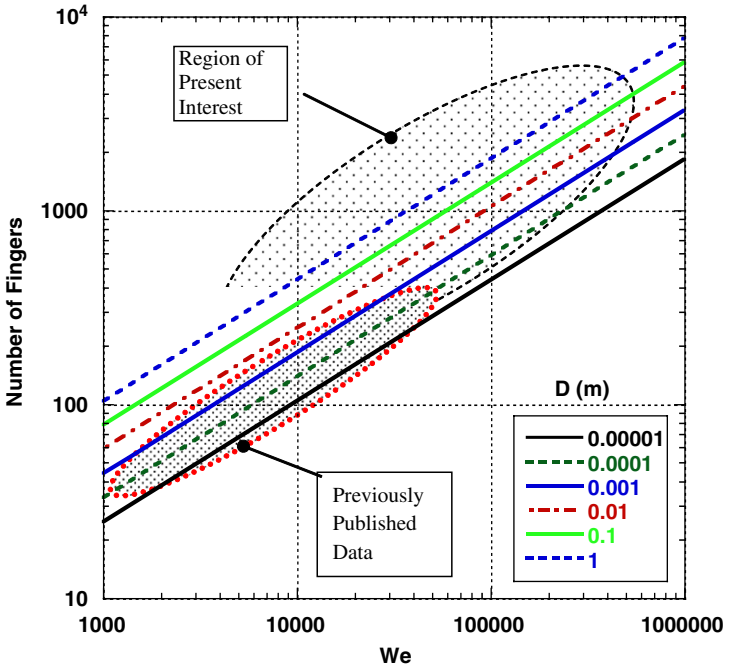

Fig. 14. Comparison between the prediction of $N_f = We^{1/2}\,Re^{1/4}/(4\sqrt{3})$, which is based on the Allen's (1975) Rayleigh–Taylor theory, and the region of the previously published experimental data for various drop sizes.

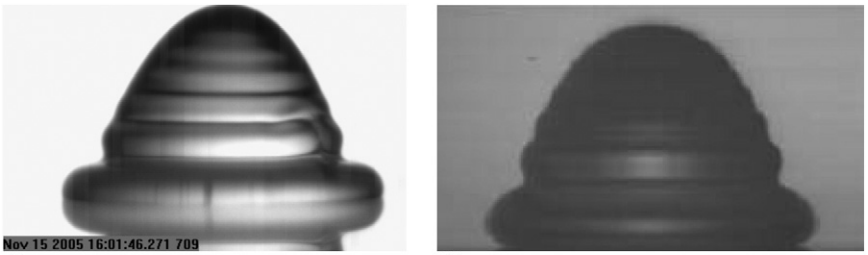

Fig. 15. Appearance of the pyramidal surface structure when We Ca < 2: (a) our current experiment: 4 mm drop with 1 m/s impact speed and (b) experimental image from Renardy et al. (2003): 1.75 mm drop at 0.41 m/s impact speed.

does not the necessary and unavoidable (for this droplet scale) initial disturbance from the bladder removal seem to affect the results at lower Weber numbers reported in the previous research? In fact, Mehdizadeh et al. (2004) did report that their experimental data deviated from the R–T prediction due to finger merging at the spreading edge, but no additional explanation for the discrepancy was given in their paper. We carefully note that the discrepancy between their experimental data and the prediction may not be because of finger merging, but because of the artifice nature of the R–T instability which reveals the dominant effect of the Weber number (over the Reynolds number) for the given small drop and high impact speed, the case considered in the prior studies. In addition, the instability that causes finger formation must not be very sensitive to the disturbances such as the formation of the "fuzzy" drop surface during the bladder removal.

Fig. 14 shows R–T predictions for various drop diameters (lines) compared with the We range of the previously published data. Most of the previous experiments dealt with smaller drop size (usually less than 5 mm) and varied the impact speed to achieve the wide range of Weber numbers. Naturally, the effect of the Weber number (proportional to $\propto U_{\mathrm{imp}}^2$) was dominant while that of the Reynolds number was small. In results, the experimental data (strongly dependent on the Weber number) and the R–T theory prediction agreed. For that matter, our data of small drop size (see Fig. 15 and the filled square symbol in Fig 13) also agree well with the R–T theory prediction. However, the comparisons are not in agreement when drop size increases. In this case, the R–T model predicts that the Reynolds number effect becomes moderately important, while the experimental data presented here and in Mehdizadeh et al. (2004) for high Weber number shows otherwise. Moreover, the R–T prediction varies significantly, by an order of magnitude, depending on the choice of the fluid acceleration. For example, the spreading liquid acceleration was approximated as $a = U_{\mathrm{imp}}^2/D_{\max}$ in Allen (1975) (where $D_{\max}$ is the maximum spreading diameter) while the acceleration was approximated as $a = U_{\mathrm{imp}}^2/D$ in Aziz and Chandra (2000). It should be noted that the ratio between $D_{\max}$ and D can increase up to $\beta_{\max} = D_{\max}/D < 12$ for the large-scale drop impact case, which is another source of substantial uncertainty.

In summary, previous tests have not compared the theory with experimental data for very large drops, the region where the validity of the R–T prediction is in question for our requirements. Also, the parameter variability of the R–T equation for predicting the finger number is too large to conclude that the R–T instability is the fundamental instability of the finger formation. There is literature indicating that the R–T model is accurate in predicting the finger number $N_{\mathrm{f}} = \mathrm{We}^{1/2}\mathrm{Re}^{1/4}/(4\sqrt{3})$ but also indicates that the experimental data on finger number is a function of the Weber number only (i.e., $N_f = 1.14\mathrm{We}^{0.5}$) (Mehdizadeh et al., 2004). Finally, the inability of the R–T instability theory to predict our dispersion characteristics is further supported by its lack of ability to support the observations in a much simpler experiment such as that shown in Xu et al. (2005) (Fig. 2) where issues with surface disturbance due to bladder removal are absent.

4. Conclusion

The experimental data presented here represent a new area of research for high-speed large liquid drop impact. This is an important area to understand because its application is of interest to civilian, military, and government agencies for safety and reliability issues in many practical applications, such as in moving vehicle collisions with flammable storage, or moving fuel-tank collisions with stationary objects. Attempts and comparisons were made to utilize current theory on drop impact and dispersion from the wide body of research on small Weber number impacts. However, the theory developed from this previous work is apparently not applicable to this new problem. In fact, the new work presented

here brings into question the R–T instability theory for all drop sizes. This is well supported by our data at comparable Weber numbers to previous work and recent research by others for drop impact at varying pressures. It is also apparent that the necessary and unavoidable delivery mechanism that causes the surface disturbance upon impact is not significant in subsequent instability and dispersion processes. Therefore, for high-speed large liquid impacts, there is a need to develop another theory or empirical relationship to describe the initial dispersion process. In conclusion, we would like to point out the two major criticisms against the conventional use of the R–T theory for explaining the liquid impact phenomenon. First, the thought of applying the R–T instability mechanism may not be correct since its prediction is contrary to the experimentally observed trend of splashing and a radially spreading droplet. Rather, the predictions of the shear-driven Kelvin–Helmholtz instability theory are in agreement with the trends of the instability mode of the splashing droplet. Second, it is perhaps naive to believe that the finger number can be predicted by the linear theory, because the later spreading motion seems to be dominated by the nonlinear behavior. This is not to say that even the Kelvin–Helmholtz linear theory is invalid for this application. We believe that the Kelvin–Helmholtz theory is indeed applicable at the early development stage of the instability, where the disturbance magnitude is moderate enough that the initial instability mode can be explained by the linear theory. It would certainly be interesting to compare the experimental data obtained in the higher gas density environment (such as argon or nitrogen) with the Kelvin–Helmholtz instability theories to ensure its applicability for the splashing droplet.

Acknowledgements

Sandia is a multiprogram laboratory operated by Sandia Corporation, a Lockheed Martin Company, for the United States Department of Energy's National Nuclear Security Administration under contract DE-AC04-94AL85000. The authors are grateful for the useful discussion shared by Dr Sheldon Tieszen and Dr John Hewson. The authors' deepest thanks go to Mr Byron Demosthenous and Mr Ed Bystrom for their constructive help with the Photometrics of the experiment. Our sincere thanks go to Prof. Sidney R. Nagel of the University of Chicago for providing the experimental images of Fig. 2. The first author wishes to acknowledge the partial support of this research by a grant R0504532 from Carbon Dioxide Reduction and Sequestration Research Center.

References

Allen, R.F., 1975. The role of surface tension in splashing. Journal of Colloid and Interface Science 51, 350–351.

Allen, R.F., 1988. The mechanics of splashing. Journal of Colloid and Interface Science 124, 309–316.

Aref, H., Tryggvason, G., 1984. Vortex dynamics of passive and active interfaces. Physica 12D, 59–70.

Aziz, S.D., Chandra, S., 2000. Impact, recoil and splashing of molten metal droplets. International Journal of Heat and Mass Transfer 43, 2841–2857.

Bussmann, M., Chandra, S., Mostaghimi, J., 2000. Modeling the splash of a droplet impacting a solid surface. Physics of Fluids 12, 3121–3132.

Chandra, S., Avedisian, C.T., 1991. On the collision of a droplet with a solid surface. Proceedings of the Royal Society of London 432, 13–41.

Chandrasekhar, S., 1961. Hydrodynamic and Hydromagnetic Stability. Oxford University Press, London.

Clark, T.T., 2003. A numerical study of the statistics of a two-dimensional Rayleigh–Taylor mixing layer. Physics of Fluids 15, 2413–2423.

Cossali, G.E., Coghe, A., Marengo, M., 1997. The impact of a single drop on a wetted solid surface. Experiments in Fluids 22, 463–472.

Davidson, M.R., 2000. Boundary integral prediction of the spreading of an inviscid drop impacting on a solid surface. Chemical Engineering Science 55, 1159–1170.

Davidson, M.R., 2002. Spreading of an inviscid drop impacting on a liquid film. Chemical Engineering Science 57, 3639–3647.

Fukai, J., Zhao, Z., Poulikakos, D., Megaridis, C.M., Miyatake, O., 1993. Modeling of the deformation of a liquid droplet impinging upon a flat surface. Physics of Fluids A 5, 2588–2599.

Ge, Y., Fan, L.S., 2005. Three-dimensional simulation of impingement of a liquid droplet on a flat surface in the Leidenfrost regime. Physics of Fluids 17, 027104.

Hansen, F.K., Rodsrud, G., 1991. Surface tension by pendant drop. Journal of Colloid and Interface Science 141, 1–9.

Jepsen, R.A., Jensen, K., O'Hern, T., 2004. Water dispersion modeling and diagnostics for water slug impact test In: SEM X International Congress.

Josserand, C., Zaleski, S., 2003. Droplet splashing on a thin liquid film. Physics of Fluids 15, 1650–1657.

Kim, H.Y., Feng, Z.C., Chun, J.H., 2000. Instability of a liquid jet emerging from a droplet upon collision with a solid surface. Physics of Fluids 12, 531–541.

Manzello, S.L., Yang, J.C., 2002. An experimental study of high Weber number impact of methoxy-nonafluorobutane $C_4F_9OCH_3$ (HFE-7100) and *n*-heptane droplets on a heated solid surface. International Journal of Heat and Mass Transfer 45, 3961–3971.

Mao, T., Kuhn, C.S., Tran, H., 1997. Spread and rebound of liquid droplets upon impact on flat surfaces. AIChE Journal 43, 2169–2179.

Marmanis, H., Thoroddsen, S.T., 1996. Physics of Fluids 8, 1344–1346.

Mehdi-Nejad, V., Mostaghimi, J., Chandra, S., 2003. Air bubble entrapment under an impacting droplet. Physics of Fluids 15, 173–183.

Mehdizadeh, N.Z., Chandra, S., Mostaghimi, J., 2004. Formation of fingers around the edges of a drop hitting a metal plate with high velocity. Journal of Fluid Mechanics 510, 353–373.

Mundo, C., Sommerfeld, M., Tropea, C., 1995. Droplet-wall collisions: experimental studies of the deformation and breakup process. International Journal of Multiphase Flow 21, 151–174.

Pasandideh-Fard, M., Qiao, Y.M., Chandra, S., Mostaghimi, J., 1996. Capillary effects during droplet impact on a solid surface. Physics of Fluids 8, 650–659.

Prosperetti, A., Oguz, H.N., 1993. The impact of drops on liquid surfaces and the underwater noise of rain. Annual Review of Fluid Mechanics 25, 577–602.

Read, K.I., 1984. Experimental investigation of turbulent mixing by Rayleigh–Taylor instability. Physica 12D, 45–58.

Rein, M., 1993. Phenomena of liquid drop impact on solid and liquid surfaces. Fluid Dynamics Research 12, 61–93.

Renardy, Y., Popinet, S., Duchemin, L., Renardy, M., Zaleski, S., Josserand, C., Drumright-Clarke, M.A., Richard, D., Clanet, C., Quere, D., 2003. Pyramidal and toroidal water drops after impact on a solid surface. Journal of Fluid Mechanics 484, 69–83.

Rieber, M., Frohn, A., 1999. A numerical study on the mechanism of splashing. International Journal of Heat and Fluid Flow 20, 455–461.

Rioboo, R., Marengo, M., Tropea, C., 2002. Time evolution of liquid drop impact onto solid, dry surfaces. Experiments in Fluids 33, 112–124.

Roisman, I.V., Rioboo, R., Tropea, C., 2002. Normal impact of a liquid drop on a dry surface: model for spreading and receding. Proceedings of the Royal Society of London A 458, 1411–1430.

Roux, D.C.D., Cooper-White, J.J., 2004. Dynamics of water spreading on a glass surface. Journal of Colloid and Interface Science 277, 424–436.

Rozhkov, A., Prunet-Foch, B., Vignes-Adler, M., 2002. Impact of water drops on small targets. Physics of Fluids 14, 3485–3501.

Sharp, D.H., 1984. An overview of Rayleigh–Taylor instability. Physica 12D, 3–18.

Sikalo, S., Marengo, M., Tropea, C., Ganic, E.N., 2002. Analysis of impact of droplets on horizontal surfaces. Experimental Thermal and Fluid Science 25, 503–510.

Sivakumar, D., Tropea, C., 2002. Splashing impact of a spray onto a liquid film. Physics of Fluids 14, L85–L88.

Thoroddsen, S.T., 2002. The ejecta sheet generated by the impact of a drop. Journal of Fluid Mechanics 451, 373–381.

Thoroddsen, S.T., Sakakibara, J., 1998. Evolution of the fingering pattern of an impacting drop. Physics of Fluids 10, 1359–1374.

Thoroddsen, S.T., Etoh, T.G., Takehara, K., Takano, Y., 2004. Impact jetting by a solid sphere. Journal of Fluid Mechanics 499, 139–148.

Weiss, D.A., Yarin, A.L., 1999. Single drop impact onto liquid films: neck distortion, jetting, tiny bubble entrainment, and crown formation. Journal of Fluid Mechanics 385, 229–254.

Worthington, A.M., 1877. On the forms assumed by drops of liquid falling on a horizontal plate. Proceedings of the Royal Society of London 25, 261.

Xu, L., Zhang, W., Nagel, S.R., 2005. Drop splashing on a dry smooth surface. Physical Review Letter 94, 184505.

Yarin, A.L., Weiss, D.A., 1995. Impact of drops on solid surfaces: self-similar capillary waves, and splashing as a new type of kinematic discontinuity. Journal of Fluid Mechanics 283, 141–173.

Youngs, D.L., 1984. Numerical simulation of turbulent mixing by Rayleigh–Taylor instability. Physica 12D, 32–44.